Sonar scattering from the sea bottom near the Norwegian coast

Jørn Inge Vestgården, Karl Thomas Hjelmervik,Dan Henrik Sekse Stender,Henrik Berg
,
Norwegian Defence Research establishment (FFI), PO Box 115, 3191 Horten, Norway

***Abstract*—High false alarm rates on active sonar systems in shallow waters is a well known problem which may be a limiting factor for the sonar performance. One way to reduce the false alarm rate is through supervised learning and machine learning algorithms applying relevant classification features. Here we propose backscatter intensity as a classification feature. It is calculated from a topographical map under the assumption of omnidirectional scattering for sound, an unrefracted path and iso-velocity sound speed profile. Analysis of historic data for a towed array sonar near the Norwegian coast showed that clutter echoes to a large extent was located at cliffs, escarpments and ridges where the calculated backscatter intensity was high. With a simple thresholding of the estimated backscatter intensity one can correctly classify 60% of terrain echoes at the expense of 10% potential target echo misclassification rate. The classification rate rises to 75% for the echoes of highest signal-to-noise ratio. The proposed classification feature is computationally inexpensive and does not depend on free parameters.**

I. Introduction

In littoral environments, low frequency, high bandwidth active sonars experience increased reverberation towards the shore [1]. This is partly due to the combination of an upsloping bottom and thinner layers of soft sediments [2]. Increased reverberation reduces detection capabilities due to a raised background level [3], but may also cause inflation of false alarms [4], [5]. Both of these effects reduce the overall sonar performance. The former effect may be predicted by inputting a detailed description of the environment in an acoustic model and use the sonar equation to estimate detection ranges. The latter effect has been investigated to some extent in literature both through acoustic modeling and statistics [5]–[7]. Today, there are readily available high resolution topographical grids and this opens for the interesting possibility of correlating the sonar contacts with topographical properties. Along these lines, a scatterer map for the Malta plateau has been made [4] and methods for identification and controlling of sonar clutter have been developed [7]. Also, detailed acoustic modeling and high-resolution terrain models have been used to predict sonar false alarm rate inflation at the upslope towards the shore [5]. In the deep sea and low frequency domain, the reverberation from the Mid-Atlantic Ridge was found to have correlations with the the sea bottom directional derivatives towards the source, given topographical map of sufficiently high resolution [8], [9].

In this work, we apply a simple scattering model inspired by optics in order to identify the strongest scattering centers, which are typically solid rock ridges and escarpments facing the source. Our model assumes omnidirectional, diffusive backscatter and the only parameter is thus the backscatter intensity, R, which is the cosine of the angle between the sea bottom normal vector and the vector to the source. The backscatter intensity is a number between zero and one, and the working hypothesis is that high R co-locates with the sonar contacts. This assumes an iso–velocity case where the transmitted signal follows a lossless, unrefracted path between the sonar and the bottom patches. While being a coarse simplification, this allows for speedy calculations that can be used for both classification purposes, but also at lower levels of sonar processing in order to reduce the false alarm rate.

The estimated backscatter intensity may be used for recognizing false alarms due to strong topographical variations, particularly upslopes. This intensity may be used as a classification feature and be combined with other features, such as statistics of kinematic track properties [10], by using a supervised learning scheme [11]. The inclusion of several different features increases the robustness of the classification scheme for instance with regards to a change of environment [12].

The working hypothesis is tested on data from the NAT III program, from 2002, where an active towed sonar array was used near the west coast of Norway. The NAT III program was a collaboration between the Dutch, French, and Norwegian Navies, as well as TNO, Thales Underwater Systems, and

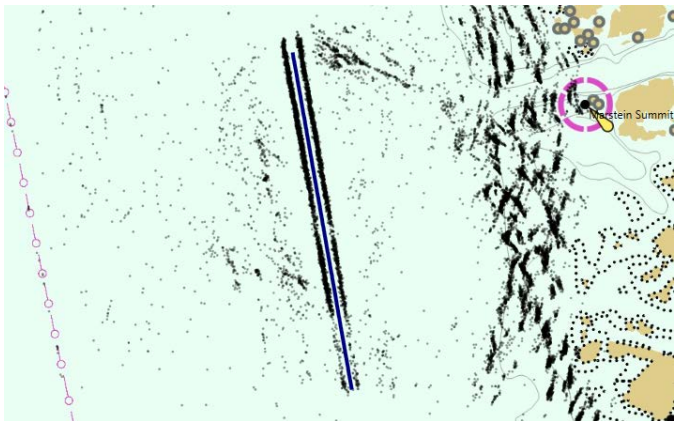

Fig. 1. The blue curve is the trajectory of the vessel sailing southwards along the Norwegian coast and black dots are echo locations. The highest concentration of echoes is at the upslope towards the shore due to sea bottom reverberation.

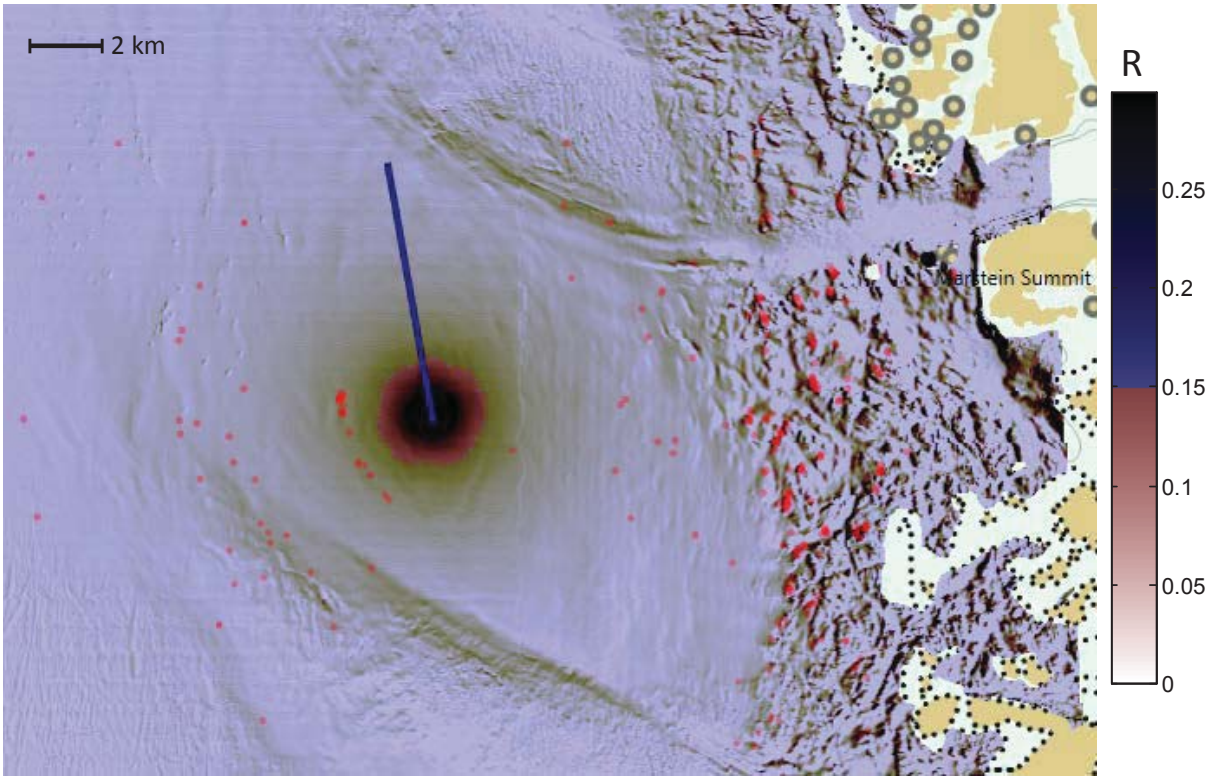

Fig. 2. The blue curve is the ship trajectory and red dots are echos from one ping. The color intensity represents R calculated based on the ping position. Most echoes appear towards the shore and high R seems to co-locate with echoes.

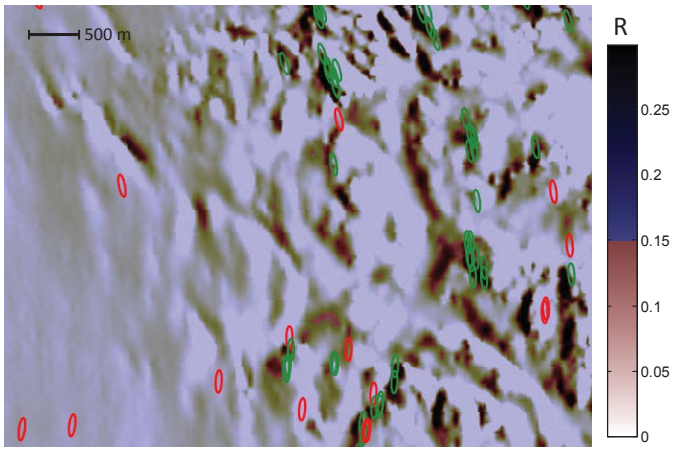

Fig. 3. Close up view of figure 2 in a region with many echoes. Green echoes are located at $R > 0.15$, red echoes at $R > 0.15$.

Norwegian Defence Research Establishment (FFI).

II. Method

The backscatter from the sea bottom is in general of a diffusive nature, which means that sound is scattered in all directions. In this work we assume omnidirectional scattering. The backscatter intensity is thus

$$R = I_0 \hat{N} \cdot \hat{r} = I_0 \cos(\alpha), \tag{1}$$

where α is the angle between the sea bottom normal $\hat{N}$ and the unit vector towards the source $\hat{r}$, and I_0 is a constant. Since we ignore transmission loss, differences in the source level, and do not distinguish between different sea bottom types, we set $I_0 = 1$. Angles $\alpha > 90°$ means sea bottom facing away from the source, and in those cases we put $R = 0$.

In order to reduce the impact of the discrete grid, the normal vector $\hat{N}$ is in every point (x, y) calculated in a coordinate frame rotated towards the source. For calculations, we use the continuous sea bottom map $z(x, y)$ calculated as a bilinear interpolation of the topographical grid. Let then $(\Delta x_1, \Delta y_1)$ be a discrete step towards the source and $(\Delta x_2, \Delta y_2) = (-\Delta y_1, \Delta x_1)$ is its transverse. The corresponding surface height differences are

$$\Delta z_1 = z(x + \Delta x_1, y + \Delta y_1) - z(x, y),$$
$$\Delta z_2 = z(x + \Delta x_2, y + \Delta y_2) - z(x, y).$$

We then have

$$\hat{N}(x, y) = \frac{(\Delta x_1, \Delta y_1, \Delta z_1) \times (\Delta x_2, \Delta y_2, \Delta z_2)}{|(\Delta x_1, \Delta y_1, \Delta z_1) \times (\Delta x_2, \Delta y_2, \Delta z_2)|}. \tag{2}$$

The discrete step $\sqrt{\Delta x_1^2 + \Delta y^2}$ is, in the calculations of this work, equals the grid spacing.

For the statistical analysis we extract distributions of R by histograms where the R interval between zero and one is divided in 20 boxes. The echo distribution $\rho_e(R)$ is calculated based on R in echo locations. The echo locations are shifted

to the bottom before R is calculated to compensate for the lack of depth information from the sonar. The background distribution $\rho_{bg}(R)$ is calculated based on a random selection of points between 1 km and 10 km from the 80 ping locations. The random points are selected with equal probability in the Cartesian grid. To minimize grid-artifacts, the R used in all calculations is the maximum value of R in the location and its four nearest neighbors.

The full dataset contains many echoes from the specular reflection from the sea bottom just below the source. Since these echoes are not the topic of our analysis, all echoes closer than 1 km are excluded from the statistical analysis.

III. Data

The second trial of the NAT III programme was carried out in September 2002. FFIs research vessel, H. U. Sverdrup II, towed an active, low-frequency array sonar system in the Norwegian Trench. CEX02 (Clutter Experiment 2) was carried out close to the shore which gives rise to many false alarms due to backscattering. An overview of the experiment can be seen in figure 1. The blue line represents the navigational path of the sonar vessel during the experiments and black dots are echoes.

The sonar system consisted of a towed body, the TNO Socrates source, and a receiver array consisting of equally spaced triplet hydrophones. The towed body was at estimated depth of 92 m and transmitted a 2 second long hyperbolic frequency modulated pulse every 90 seconds. The transmission period was two hours, with a total of 80 transmissions.

In order to calculate the scattering strength a topographical grid with sufficient resolution is required. This work is based on data from the Norwegian Mapping Authority in UTM projection with grid spacing of 50 m.

IV. Results

Figure 2 shows the echoes from ping number 34. The source is in the Norwegian Trench, 15 km west of Marstein summit, where the sea bottom is relatively flat and sea depth is typically 300 m. This ping resulted in 254 echoes, with the majority located in the upslope towards the shore. The color intensity represents R calculated with $\hat{r}$ pointing towards the source. The map shows that in the east, towards the shore, the topography is varied and the map has a rich set of features, with a landscape-like appearance. In particular, we notice the typical high R regions are extending from north to south, transverse to the source. These regions are a few hundred meters wide and the length is up to several kilometers. Most likely these are escarpments facing the source. Echoes are often found at or near these high R structures. Even though the connection between high R and echo locations is not absolute, the connection appears to be strong enough to be used as a statistical classification feature.

Focusing instead on the flat area in the central and western part of figure 2, R is moderate, typically with $R < 0.15$, yet with some fine structure. There are also some echoes, but there seems to be no correspondence between the structure of

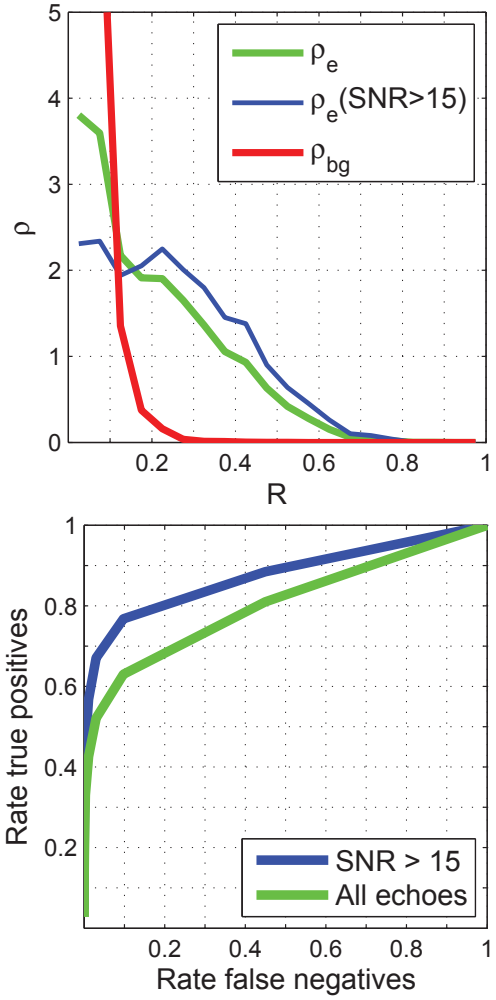

Fig. 4. Top: Distribution of R at random locations within the sonar range (red), and at all echo locations (green), and at echo locations with SNR>15 (blue). Bottom: ROC curves weighting the rates of true posties and false negatives.

the R map and the echo locations, indicating that sea bottom scattering is not the source of these echoes.

Figure 3 shows a close up view of the echo locations and R-map in the steeper regions where there are many echoes. The echoes are color coded so that green and red means $R > 0.15$ and < 0.15, respectively. The size of the ellipse is arbitrary and does not reflect the sonar uncertainty. The figure shows that the echoes often co-locate with high R values. Other echoes are sufficiently close to areas with high R that it is plausible that the difference is due to the localization uncertainty of the sonar system. The lack of echoes in some of the places with high R can be explained by the sonar blind zones, but in order to verify this we need to apply a full acoustical model.

The top panel of figure 4 shows the distributions of R at echo locations, ρ_e, for all echoes and echoes with SNR > 15 dB, and the background distribution ρ_{bg}. The background distribution is calculated from R in 62135 randomly selected locations within the sonar range. The distribution is a monotonically decreasing function with most values below 0.15 and

it approaches zero at 0.3. The echo distributions are highly different. They also have a peak at zero, but they fall off much more slowly, with many values also in the range between 0.15 and 0.8. The distribution based on R on 9628 echoes with SNR > 15 dB is shifted towards higher values than the distribution based on all 33056 echos. This indicates that backscatter from terrain yield higher SNR than other sources of false alarms.

The bottom panel of figure 4 shows ROC curves weighting the rate of true positives and rate of false negatives for all echoes and echoes with SNR > 15 dB. A true positive is a correctly classified terrain-echo, whereas a false negative is a random location classified as terrain. The unconventional choice of weighting towards false negatives is justified by our intention of removing true positives to clarify the sonar picture. The ROC curve is thus interpreted as a conventional ROC curve where the optimal point is $(0, 1)$ and curves above the diagonal signal a useful feature, with more true positives than false negatives. The ROC curves rise very sharply and it seems that it is possible to remove 40% of all echoes and 60% of echoes with SNR > 15dB with hardly any false negatives. With 10% rate of false negatives, the corresponding rates of true positives are 60% and 75%. This corresponds to a R-threshold of 0.13. The threshold $R = 0.15$ implies a rate of false negatives of 5%. In total, the statistical analysis implies that a great simplification of the sonar picture is possible in littoral waters where the dominant mechanism for creation of false alarms is sea bottom reverberation.

V. Discussion

The model of this work deviates from models used in the literature where reverberation strength has been quantified by directional derivatives [8], [9], depth-weighted topographic slope [7], or a ray-tracer acoustic model [5]. The main benefit of the proposed model is its simplicity. Yet, a full acoustical model is likely to improve the results, at the expense of increased computation time and introduction of unknown parameters. The most obvious improvements is to identify sonar blind zones, bending of rays due to sound speed variations, transmission loss, and multipath contributions. The sea bottom properties will also be of importance, since the backscatter from rock is typically orders of magnitude higher than from sand and mud.

In the analyzed data, the source was at 92 m, whereas the maximum depth is approximately 300 m. This means that, for the iso–velocity case, the transmission beam makes at most 12° and 2° with a flat bottom at 1 km and 10 km, respectively. This gives $R = 0.2$ and $R = 0.02$ in the two cases. The typically used cutoff of $R = 0.15$ corresponds to a flat bottom at 1400 m. The dependence of distance indicates that statistics should also take into account distance to avoid misclassification close to the source.

The distribution of R at echo locations are typically below 0.6. To get a feeling of what kind of terrain features that give rise to echoes, let us assume a horizontal beam. Then, the values for $R = 0.2$, 0.4 and 0.6 correspond to terrain with grazing angles 12°, 24°, and 37°, respectively. The escarpments giving rise to echoes are rather steep, and it is thus likely they will constitute of rock.

VI. Conclusion

We have considered sea bottom scattering strength as a classification feature for sonar echoes. The scattering strength was quantified by the cosine of the angle between the sea bottom normal and the direction towards the source, assuming an straight, unrefracted, single path of propagation to the source. The main application of the method is to classify terrain echoes so that sonar operators can be presented with a sonar picture with a reduced false alarm rate.

Due to the disregarding of propagation loss and sound ray bending the model is mainly suited for shallow waters where the direct path contributions are dominant. Thus, the model has been tested on a historic dataset of towed array sonar near the Norwegian coast, where sea depth is below 300 m. The results show that it is possible to correctly classify up to 60% of terrain echoes at the expense of 10% potential target echo misclassification rate. For echoes with SNR above 15 dB, the classification rate rises to 75%, indicating that sea bottom reverberation echoes have higher SNR than other sources of false alarms.

The conclusions are based on just one historic dataset, which was specifically performed to induce a high level terrain echoes. It is likely that the method will work also in other environments with a high number of terrain echoes, say inside fjords, but further tests are needed to verify this. The background distribution can readily be calculated given just the sailing route and estimated sonar range. In order to obtain echo distributions one has to perform actual tests, and it is likely that the echo distribution will vary with environment and sonar type and settings.

Acknowledgment

The data of this work was obtained by a collaboration between FFI, TNO, Thales Underwater Systems, and the Dutch, French and Norwegian navies. The sonar processing was carried out by TNO.

References

[1] N. Chotiros, H. Boehme, T. Goldsberry, S. Pitt, R. Lamb, A. Garcia, and R. Altenburg, "Acoustic backscattering at low grazing angles from the ocean bottom. part ii. statistical characteristics of bottom backscatter at a shallow water site," *The Journal of the Acoustical Society of America*, vol. 77, no. 3, pp. 975–982, 1985.

[2] A. A. Søvik and K. T. Hjelmervik, in *IEEE proceedings of Oceans, Aberdeen*. IEEE, 2017.

[3] R. J. Urick, *Principles of underwater sound for engineers*. Tata McGraw-Hill Education, 1967.

[4] M. K. Prior, "A scatterer map for the malta plateau," *Oceanic Engineering, IEEE Journal of*, vol. 30, no. 4, pp. 676–690, 2005.

[5] K. T. Hjelmervik, "Predicting sonar false alarm rate inflation using acoustic modeling and a high-resolution terrain model," *Oceanic Engineering, IEEE Journal of*, vol. 35, no. 2, pp. 278–287, 2010.

[6] A. P. Lyons and D. A. Abraham, "Statistical characterization of high-frequency shallow-water seafloor backscatter," *The Journal of the Acoustical Society of America*, vol. 106, no. 3, pp. 1307–1315, 1999.

[7] J. M. Fialkowski and R. C. Gauss, "Methods for identifying and controlling sonar clutter," *IEEE Journal of Oceanic Engineering*, vol. 35, no. 2, pp. 330–354, 2010.

[8] N. C. Makris and J. M. Berkson, "Long-range backscatter from the Mid-Atlantic Ridge," *The Journal of the Acoustical Society of America*, vol. 95, no. 4, p. 1865, 1993.

[9] ——, "Deterministic reverberation from ocean ridges," *The Journal of the Acoustical Society of America*, vol. 97, no. 6, p. 3547, 1995.

[10] D. H. S. Stender, K. T. Hjelmervik, H. Berg, and T. S. Såstad, "Assessing the performance of kinematic track features for classification of sonar targets in anti-submarine warfare," in *UDT Europe 2016-Conference Proceedings Undersea Defence Technology, 1-3 June 2016, Lillestrom, Norway*. Clarion Events Ltd, 2016.

[11] H. Berg, K. T. Hjelmervik, D. H. S. Stender, and T. S. Såstad, "A comparison of different machine learning algorithms for automatic classification of sonar targets," in *Oceans 2016 - Monterey*. IEEE, 2016.

[12] D. H. S. Stender, H. Berg, K. T. Hjelmervik, and T. S. Såstad, "The classification performance of signal-to-noise ratio and kinematic features in varying environments," in *IEEE proceedings of Oceans, Aberdeen*. IEEE, 2017.